



 Cite this: *New J. Chem.*, 2023, 47, 11557

# A novel carbazole-benzothiazole-based chemodosimeter for the chromogenic and fluorogenic recognition of $\text{CN}^-$ †

 Atanu Maji, Amitav Biswas, Akash Das, Saswati Gharami, Krishnendu Aich and Tapan K. Mondal \*

A novel colorimetric and fluorescent sensing probe, (*E*)-3-(4-(9H-carbazol-9-yl)phenyl)-2-(benzo[*d*]thiazol-2-yl)acrylonitrile (CBTA), was synthesized and characterized by spectroscopic techniques. CBTA displayed “turn off” fluorescence in the presence of cyanide with a higher selectivity than that of others anions such as  $\text{Br}^-$ ,  $\text{Cl}^-$ ,  $\text{I}^-$ ,  $\text{NO}_3^-$ ,  $\text{SO}_4^{2-}$ ,  $\text{SCN}^-$ ,  $\text{CO}_3^{2-}$ ,  $\text{N}_3^-$ ,  $\text{OH}^-$ ,  $\text{HCO}_3^-$ ,  $\text{H}_2\text{PO}_4^-$ ,  $\text{HPO}_4^{2-}$ ,  $\text{F}^-$ ,  $\text{ACO}^-$ , and  $\text{PO}_4^{3-}$  in a DMSO:H<sub>2</sub>O medium (40:60, v/v, HEPES buffer, pH = 7.2). The “turn off” fluorescence response mechanism can be attributed to the intra-molecular charge transfer (ICT) process, which is blocked by the nucleophilic attack of cyanide ions at the cyano vinyl group of the probe. The LOD was found to be  $3.57 \times 10^{-8}$  M. The interaction involved behind the sensing of cyanide was investigated by Job’s plot analysis, <sup>1</sup>H-NMR, and mass spectroscopic studies. DFT and TDDFT were also employed to verify the experimental outcomes. Moreover, the test strip experiment provides a wide application prospect of the receptor for detecting poisonous cyanide in the environment and biological system.

 Received 11th March 2023,  
 Accepted 17th May 2023

DOI: 10.1039/d3nj01157g

rsc.li/njc

## Introduction

The development of a new molecular probe for the detection of anions is of great interest because of their vital roles in a wide range of medicines, catalysis, life science, and environment.<sup>1</sup> Additionally, food safety issues and water pollution by poisonous anions have drawn attention with the development of science and technology nowadays.<sup>2–6</sup> Cyanide is one of the most well-known toxic anions, even at a lower concentration, which can be lethal to human beings, animals, and environment. Cyanide is currently extensively used in many industrial processes such as electroplating, petrochemicals, photography, steel production, gold mining, metallurgy, and the synthesis of resin and fibre due to its critical role in multi-functional reactions.<sup>7</sup> World Health Organization (WHO) stipulates that the permissible acceptable concentration of cyanide in drinking water is  $1.9 \times 10^{-6}$  mol L<sup>-1</sup>.<sup>8</sup> By the way, cyanide is present in some insects, fruits, seeds, and roots where it is released through the hydrolysis process of cyanogenic glycosides.<sup>9–14</sup> Cyanide binds to the iron ion in cytochrome *c* oxidase, blocks the electron transport in metabolism, and inhibits the

production of ATP in cells, making the biological system inefficient to provide sufficient energy to the heart, central nervous system and other vital organs ultimately.<sup>15,16</sup> Considering the above-mentioned fact, the development of simple, efficient and rapid detection tools with high selectivity and sensitivity towards cyanide is an ongoing hot topic to prevent the harmful effect in the human body from contaminated food and environment.

To date, fluorescent molecular probes capable of detecting  $\text{CN}^-$  have been reported based on fluorescence resonance energy transfer (FRET),<sup>17–19</sup> intra-molecular charge transfer (ICT),<sup>20,21</sup> twisted intra-molecular charge transfer (TICT),<sup>22</sup> excited state intra-molecular proton transfer (ESIPT),<sup>23,24</sup> and photo-induced electron transfer (PET).<sup>25,26</sup> Recently, several groups have reported detection methods by utilizing the nucleophilic addition reaction of cyanide directly involved in the development of covalent bond formation and showed anti-interference ability and high selectivity.<sup>27–38</sup> Compared with the traditional sophisticated analytical tools such as spectrophotometry, voltammetry, chromatography, and potentiometric methods, optical molecular probes based on colorimetric and fluorometric responses towards  $\text{CN}^-$  are of great preference in virtue of their convenience, simplicity, tenability, low cost, high selectivity and rapid response.<sup>39</sup> Particularly, a naked-eye optical sensor is very much impressive. Since the Tang *et al.* discovery of the AIE phenomenon in 2001, several research groups have been published a growing number of AIE active

Department of Chemistry, Jadavpur University, Kolkata-700032, India.

E-mail: tapank.mondal@jadavpuruniversity.in

 † Electronic supplementary information (ESI) available: NMR and MS of all new compounds, limit of detection determination, quantum yield calculation. See DOI: <https://doi.org/10.1039/d3nj01157g>

fluorescent probes<sup>47–50</sup> for their wide application in optoelectronics, environmental monitoring, biological imaging as well as in the construction of the green energy devices and chemosensors.<sup>39–46</sup> The active AIE effect is mainly due to the restriction of molecular motion. Therefore, the fabrication of AIE active fluorescent probes for the recognition of  $\text{CN}^-$  in an aqueous medium is now a recent trend depending on the special features of AIE active molecules.<sup>51,52</sup> Thus far, with the developed intra-molecular charge transfer (ICT) process, plenty of typical donor- $\pi$ -acceptor (D- $\pi$ -A) type sensors have been reported to recognize trace  $\text{CN}^-$  ions, which inhibit the ICT process by nucleophilic attack at the subunits (such C=C and C=N) and causes obvious color and spectral changes.<sup>53–65</sup> Keeping in mind the unique nucleophilicity of  $\text{CN}^-$  ions, cyanide can be recognized by the donor- $\pi$ -acceptor (D- $\pi$ -A)-type molecular probe considered as a colorimetric and fluorimetric sensor.

In this work, we successfully fabricated an AIE active chemodosimeter (CBTA; Scheme 1) consisting of a donor- $\pi$ -acceptor (D- $\pi$ -A) skeleton in which carbazole acts as a donor moiety and benzothiazole acts as an acceptor unit. The probe can be used as a new dual-modal colorimetric and fluorescent sensor for distinct detection of cyanide ions among all other relative anions based on the ICT mechanism and exhibited high sensitivity and selectivity in 60% aqueous DMSO solution. The sensing mechanism could be ascribed to the nucleophilic attack by the cyanide ion to the vinyl group of the receptor that leads to the cut off in the ICT process, causing the spectroscopic changes followed by the obvious color changes that could be distinguished by the naked eye in the ambient light as well as under a UV lamp.

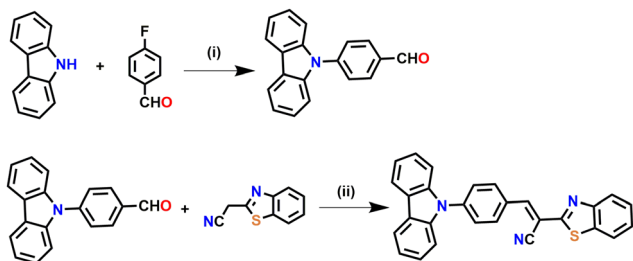
## Results and discussion

### Synthesis of the probe (CBTA)

The chemodosimeter (CBTA) was synthesized *via* the condensation of 4-(9H-carbazol-9-yl)benzaldehyde and 2-(benzo[*d*]thiazol-2-yl)acetonitrile in an absolute ethanol solvent under reflux conditions (Scheme 1). The chemical structure of CBTA has been confirmed by <sup>1</sup>H-NMR, <sup>13</sup>C-NMR, IR-spectroscopy, and mass-spectral analysis (Fig. S1–S4, ESI<sup>†</sup>).

### Aggregation-induced emission enhancement (AIEE) effect of CBTA

AIEE behavior of CBTA was studied by fluorescence spectra. As water is an undesirable solvent, the addition of  $\text{H}_2\text{O}$  to DMSO



**Scheme 1** Synthetic route of the probe, CBTA. (i) KOtBu, DMF, 100 °C, 12 h; (ii) EtOH, piperidine, reflux, 7 h.

facilitates the aggregation of CBTA. The fluorescence changes of CBTA are shown by modifying the DMSO to water proportion in the solvent system. The fluorescence intensity gradually decreases as the volume proportion of water of the  $\text{H}_2\text{O}$ -DMSO solution increases from 0% to 40%. After that, a dramatic enhancement in the fluorescence intensity was observed and the maximum intensity was achieved at 60% of water content with a red shift of 16 nm along with large enhancement of the fluorescence intensity by about 6 fold compared to the fluorescence intensity in a pure DMSO solvent (Fig. 1). It is suggested that the aggregation of the probe, CBTA, started after about 40% of water fraction in solvent situation. All these findings show that our probe is AIEE active. The free intra-molecular single bond rotation in the free probe that quenches the emission intensity *via* non-radiative decay is responsible for not viewing AIEE activity in the solution phase. However, in the aggregate state where this rotation is forbidden, high fluorescence intensity with a red shift is displayed. The large enhancement in fluorescence intensity with a red shift may be ascribed to the electronic transition ( $\pi$ - $\pi^*$ ) inside the probe.

### Sensing performance of CBTA

**Selectivity and anti-interference of anions.** In order to observe the sensing ability of CBTA, the UV-vis spectra of the probe were recorded in the presence and absence of various chosen anions ( $\text{F}^-$ ,  $\text{Cl}^-$ ,  $\text{ACO}^-$ ,  $\text{NO}_3^-$ ,  $\text{SCN}^-$ ,  $\text{CO}_3^{2-}$ ,  $\text{HCO}_3^-$ ,  $\text{HSO}_4^-$ ,  $\text{SO}_4^{2-}$ ,  $\text{H}_2\text{PO}_4^-$ ,  $\text{HPO}_4^{2-}$ , and  $\text{CN}^-$ ) in a DMSO- $\text{H}_2\text{O}$  (40:60, v/v, HEPES buffer, pH = 7.2) solution at room temperature. Upon addition of  $\text{CN}^-$ , the solution color changes instantly from yellow to colorless in ambient light (Fig. S15(a), ESI<sup>†</sup>). Furthermore, an intense bright orange-yellow fluorescence change to light blue was clearly observed by naked eye after addition of a  $\text{CN}^-$  solution under a UV lamp, which is noticeably different from that orange-yellow fluorescence upon addition of several anions (Fig. S15(b), ESI<sup>†</sup>). Fig. S5 and S4 (ESI<sup>†</sup>) display the absorption and emission spectra of CBTA upon addition of various chosen anions respectively. As shown in Fig. S5 (ESI<sup>†</sup>),

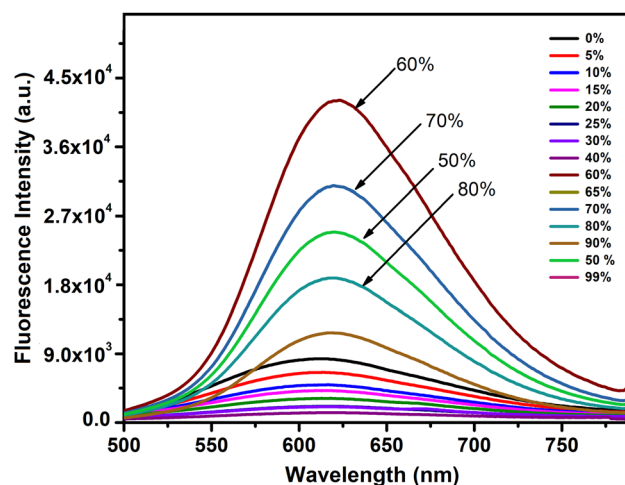


**Fig. 1** Emission spectra of CBTA (20 μM) in DMSO/water mixtures (v/v) with different water fractions ( $f_w$ ) (excitation = 409 nm).

the probe shows an absorption band at 410 nm along with two small humps at 339 nm and 293 nm in the absorption spectrum of CBTA. The absorption peaks at 293 and 339 nm are attributed to the local  $\pi-\pi^*$  electronic transition inside the probe, while the one at 410 nm may be accredited due to the intramolecular charge transfer (ICT) process from the carbazole moiety to the electron deficient benzothiazole units. Upon gradual addition of  $\text{CN}^-$ , the absorption peaks at 293 nm and 410 nm are decreased along with the appearance of a new peak at 353 nm. However, upon addition of the other anions except  $\text{CN}^-$ , the absorption spectra remain almost unaltered relative to that of the free receptor. The spectral data are in good agreement with the phenomenon shown in Fig. S15(a) (ESI<sup>†</sup>). The fluorescence spectra of CBTA show an emission peak at 616 nm upon excitation at 407 nm, which is assigned to the ICT process (Fig. 4). Upon addition of each chosen anions (2.0 equiv.) except for  $\text{CN}^-$ , only negligible change is noticed in the fluorescence spectra (Fig. 4). However, the fluorescence intensity at 616 nm remarkably quenched upon addition of  $\text{CN}^-$ , which indicates that the ICT process is inhibited due to the nucleophilic attack by  $\text{CN}^-$ . These results supported that CBTA can be used as a simple 'turn-off' sensor for naked-eye recognition and fluorescent monitoring of  $\text{CN}^-$  in 60% aqueous DMSO solution.

**Detection performance of sensor CBTA to  $\text{CN}^-$ .** The changes in the absorption spectra of CBTA after addition of  $\text{CN}^-$  at different concentrations were recorded in 60% aq. DMSO solution (Fig. 2). In the absorption spectral changes, it is clearly observed that the absorption bands at 293 nm, 339 nm and 410 nm consecutively attenuate along with a progressive raise of a new absorption peak at 358 nm upon successive addition of  $\text{CN}^-$  (0–2 equiv.). Upon incremental addition of  $\text{CN}^-$ , the emission band at 616 nm decreases gradually along with the appearance of a small new emission band at 512 nm upon excitation at 407 nm (Fig. 3), suggesting that CBTA could be served as a potential candidate to quantitatively monitor  $\text{CN}^-$  ions. To illustrate the efficiency and selectivity of the present probe (CBTA) towards  $\text{CN}^-$  ions, the limit of detection (LOD) of

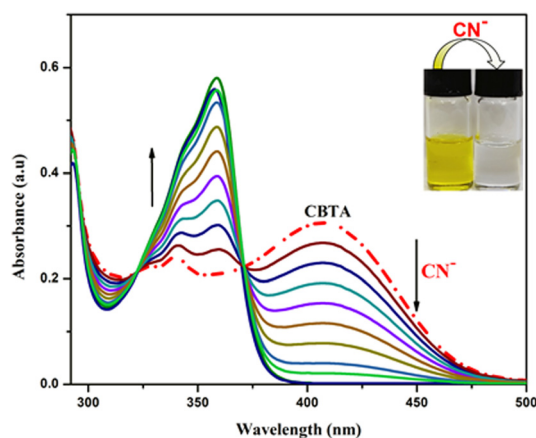


Fig. 2 Change in the UV-Vis spectrum of CBTA (20  $\mu\text{M}$ ) upon addition of  $\text{CN}^-$  (40  $\mu\text{M}$ ) in DMSO/ $\text{H}_2\text{O}$  (40 : 60, v/v) (HEPES buffer, pH = 7.2). (Inset shows the change in colour in sunlight).

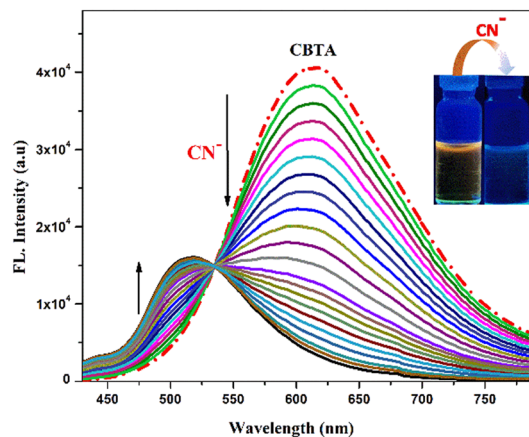


Fig. 3 Change in the emission spectra of CBTA (20  $\mu\text{M}$ ) upon gradual addition of  $\text{CN}^-$  (40  $\mu\text{M}$ ) in DMSO/ $\text{H}_2\text{O}$  (40 : 60, v/v) (HEPES buffer, pH = 7.2). (Inset shows the change in colour under UV irradiation.)

the probe for cyanide ions was calculated to be  $(7.68 \pm 0.29) \times 10^{-8}$  (M), which was established from the fluorescence titration data of the CBTA upon addition of  $\text{CN}^-$  using the equation,  $\text{LOD} = K \times (\text{SD}/S)$ , where SD and  $S$  stand for the standard deviation and the slope of the linear response curve respectively (Fig. S7, ESI<sup>†</sup>). From the mole ratio plot of CBTA, it can be stated that after addition of almost 7  $\mu\text{M}$  of  $\text{CN}^-$ , no significant changes in emission intensity at 616 nm is displayed, thereby signifying to the fact that the saturation has taken place (Fig. S18, ESI<sup>†</sup>). In addition, the kinetics study was also performed to monitor the reaction time of the probe with  $\text{CN}^-$  and fluorescence spectra were recorded depending on time. This experiment shows that the fluorescence intensity of the probe at 616 nm and absorbance at 410 nm rapidly decreases as the reaction progresses and CBTA- $\text{CN}^-$  adduct forms and finally reaches its minimum and stable value within 22 s, indicating the completion of the reaction (Fig. 5). These observations clearly suggest that cyanide can result in the color change of CBTA solution as well as the attenuation of fluorescence intensity, implying CBTA may be used as a potential candidate in a portable device for rapid  $\text{CN}^-$  recognition.

**Competitive study.** To confirm the specific selectivity of CBTA to  $\text{CN}^-$ , a competition experiment was executed upon addition of  $\text{CN}^-$  to CBTA solution containing other common anions in DMSO/ $\text{H}_2\text{O}$  (40 : 60, v/v). As observed in Fig. 6, it is almost unchanged in  $\text{CN}^-$ -induced fluorescence intensity in the presence of all other anions, which can also be referred as a binary competitive system "target + anion" in the same solution phase, indicating efficient  $\text{CN}^-$  signalling aptitude and higher anti-interference capability of the CBTA- $\text{CN}^-$  system.

**pH study.** To investigate the dependence of CBTA towards pH, we recorded the emission spectra of CBTA and CBTA- $\text{CN}^-$  in a DMSO- $\text{H}_2\text{O}$  (40 : 60, v/v) solution with different pH values (2.0–12.0). For the free receptor, the emission of the solution remains almost unaltered within the pH range of 0 to 9, and after that, emission intensity slightly decreases with the increase in pH. The maximum emission quenching of CBTA in the presence of  $\text{CN}^-$  ions was observed at pH 7.2, suggesting

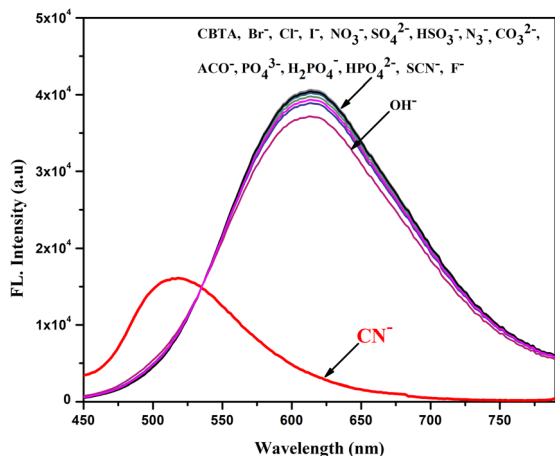


Fig. 4 Change in the emission spectrum of CBTA (20  $\mu\text{M}$ ) upon addition of different anions (40  $\mu\text{M}$ ) in a DMSO–H<sub>2</sub>O (40 : 60, v/v, HEPES buffer, pH = 7.3) solution.

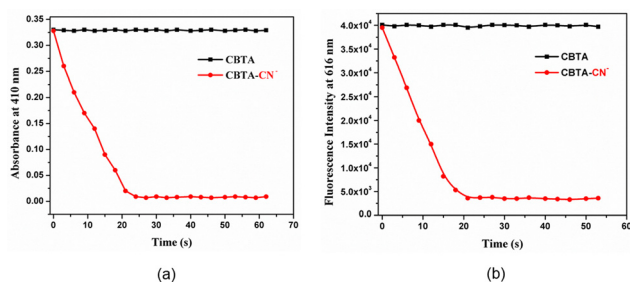


Fig. 5 Time-dependent absorbance (a) and fluorescence spectrum (b) of CBTA towards  $\text{CN}^-$  in DMSO–H<sub>2</sub>O (40 : 60, v/v, pH = 7.2).

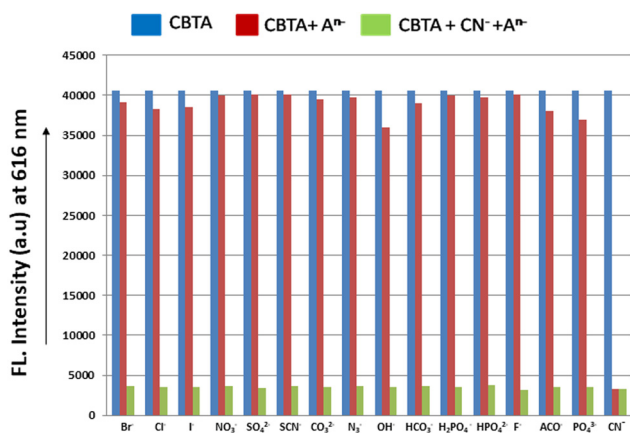


Fig. 6 Competitive experiments of CBTA (20  $\mu\text{M}$ ) for  $\text{CN}^-$  (40  $\mu\text{M}$ ) in the presence of common anions (40  $\mu\text{M}$ ) in a 60% aqueous DMSO mixture.

that the probe is suitable to show maximum sensing ability under neutral pH conditions (Fig. S8, ESI<sup>†</sup>).

**TRPL study.** Time-resolved fluorescence technique (TRPL) was also studied to examine the excited state behaviour of the fabricated probe (CBTA) and the cyanide adduct (CBTA–CN).

The fluorescence decay curves of CBTA and cyanide adduct are obtained by using the mono-exponential functions with good  $\chi^2$  values (Fig. S9, ESI<sup>†</sup>). For CBTA,  $\tau = 6.1$  ns ( $\chi^2 = 1.16$ ), and for the CBTA–CN adduct,  $\tau = 1.38$  ns ( $\chi^2 = 1.14$ ). Radiative rate constant  $K_r$  and total non-radiative rate constant  $K_{nr}$  have been calculated using the equation  $\tau^{-1} = K_r + K_{nr}$  and  $K_r = \phi_f/\tau$  (Table S2, ESI<sup>†</sup>). The change in the value of  $\tau$ ,  $K_r$  and  $K_{nr}$  supports the adduct formation of  $\text{CN}^-$  with the probe CBTA to form a new very weak fluorogenic compound CBTA–CN, which has lower life-time than the free probe itself.

**Probable sensing mechanism.** The possible interaction mechanism of the probe, CBTA, towards  $\text{CN}^-$  was investigated by <sup>1</sup>H-NMR spectroscopy. In the <sup>1</sup>H-NMR spectrum of free CBTA, the resonance signal of aromatic protons appears at around 8.42–7.35 ppm (16H), whereas after addition of 1.0 equivalent of  $\text{CN}^-$ , the protons shifted to an upfield region at around 7.88–6.81 ppm (16 H) due to the development of negative charge in the CBTA–CN adduct, clearly indicating the break-down of conjugation between benzothiazole and phenyl carbazole units. However, in the resonance spectra of CBTA–CN adduct, the proton signal at 8.57 ppm, corresponding to the vinylic proton in the free CBTA, disappeared together with the appearance of a new upfield signal at around 5.43 ppm (Fig. 8), which confirms the formation of the CBTA–CN adduct. The formation of CBTA–CN-species is also supported by HRMS spectroscopy. The mass spectrum shows a peak at 428.12 ( $m/z$ ) that corresponds to the probe itself (Fig. S3, ESI<sup>†</sup>). However, a new peak at 455.13 ( $m/z$ ) confirms the formation of CBTA–CN adduct (Fig. S17, ESI<sup>†</sup>). In addition, the estimation of the exact stoichiometry of the adduct formation, Job's plot analysis was carried out. The minimum intensity showed 0.5 mole fraction of  $\text{CN}^-$ , indicating 1 : 1 adduct formation of CBTA with  $\text{CN}^-$ , which is also supported by the observed peak at 455.13 ( $m/z$ ) in the mass spectroscopy of the adduct (Fig. S17, ESI<sup>†</sup>). These outcomes reveal the nucleophilic addition of cyanide at the cyano vinyl position accompanied by the conversion of  $\text{sp}^2$  hybridized carbon to  $\text{sp}^3$  hybridization (Fig. 7).

#### Dip-stick experiment: detection of $\text{CN}^-$ using a TLC plate

For visual detection of  $\text{CN}^-$  ions, we have performed a proficient portable method called dip-stick in which the probe can act as a fluorescent portable kit showing its sensing property towards  $\text{CN}^-$  in solid state too. Therefore, to execute this experiment, few thin-layer chromatography (TLC) plates were prepared and they were dipped into a CBTA solution ( $2 \times 10^{-4}$  M) in DMSO and then kept for some time so as to evaporate the solvent in air.

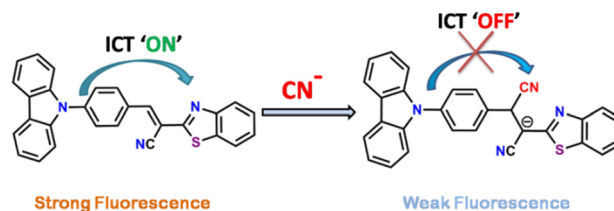


Fig. 7 Proposed sensing mechanism of CBTA with  $\text{CN}^-$ .

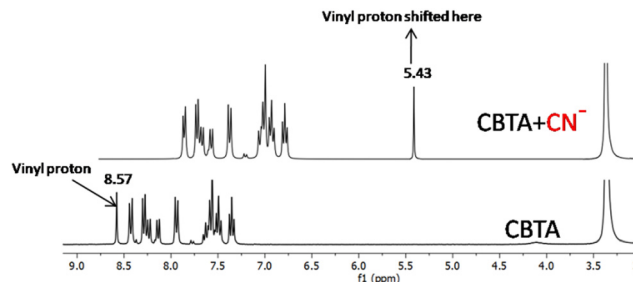


Fig. 8  $^1\text{H-NMR}$  spectrum of CBTA and CBTA- $\text{CN}^-$  in  $\text{DMSO-d}_6$ .

A fluorescence colour change observed when strips are immersed into an aqueous solution ( $2 \times 10^{-3}$  M) of cyanide and dried. This colour change can be easily visualised by naked eyes when exposed in ambient light as well as under UV light (Fig. 9). As  $\text{CN}^-$  shows different colours under UV light upon reaction with the receptor (CBTA) present in the test strips, we can easily distinguish it qualitatively. We have also demonstrated the colorimetric responses of CBTA-coated test strips induced by different concentrations of  $\text{CN}^-$  (Fig. 10) in ambient light and under UV-light.

#### Photosensitivity study

For fluorescence-based detection application, a sensor having high photo-stability with displaying steady analytical signals is highly desirable. Therefore, in order to photostability evaluations, sensor CBTA and CBTA- $\text{CN}^-$  adducts were used over 60 min in day light under optimal conditions according to the previously reported procedure.<sup>66</sup> As depicted in Fig. S10 (ESI<sup>†</sup>), sensor CBTA and CBTA- $\text{CN}^-$  adducts have highly photostable relative fluorescence responses throughout the experimental time (60 min) with slight signal change. This experimental results shows that receptor CBTA has a highly photostable “turn-off” fluorescence signal response after nucleophilic addition of  $\text{CN}^-$ , making it compatible for the spectrofluorimetric analysis of real samples.

#### Real sample analysis

As cyanide from different sources could possibly be dumped into water and pollute the water resources, it is highly urgent to detect the concentration level in these wastewater. In order to

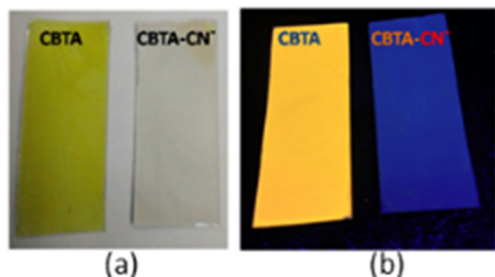


Fig. 9 Pictures of TLC plates after immersion in 60% (v/v) aqueous DMSO solution of CBTA and in CBTA- $\text{CN}^-$  under sunlight (a) and UV chamber (b).  $[\text{CBTA}] = 2 \times 10^{-4}$  M,  $[\text{CN}^-] = 2 \times 10^{-3}$  M. Excitation wavelength of the UV light is 380 nm.

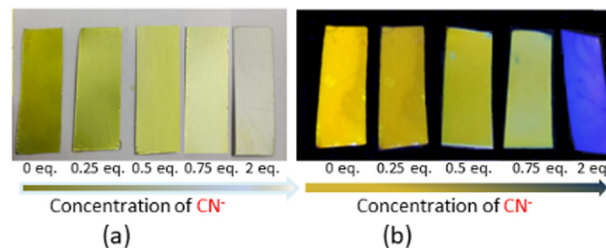


Fig. 10 Pictures of TLC plates after immersion in 60% (v/v) aqueous DMSO solution of CBTA in the presence of different  $\text{CN}^-$  concentration under sunlight (a) and UV chamber (b).  $[\text{CBTA}] = 2 \times 10^{-4}$  M,  $[\text{CN}^-] = 2 \times 10^{-3}$  M. Excitation wavelength of the UV light is 380 nm.

validate the practicality of our approach, we have analyzed natural water resources (tap, pond, river) for the sensing of  $\text{CN}^-$  according to the previously reported procedure.<sup>67–71</sup> As shown in Table 1, cyanide in these natural water resources were not measured. Then different concentrations of cyanide ions were added into these natural water samples and the sensor CBTA was employed to recover the concentrations of cyanide. From Table 1, it is concluded that the probe is highly efficient to detect the concentration of cyanide from contaminated water samples with good recovery (97–100.5%). Therefore, this experiment established that our probe CBTA is capable of determining cyanide concentration levels quantitatively in the natural water resources.

#### Computational study

In order to interpret the interaction mechanism of the chemodosimeter (CBTA) for the recognition of  $\text{CN}^-$ , geometry optimization of CBTA and CBTA- $\text{CN}^-$  was performed by the DFT/B3LYP/6-31+G(d) method using the Gaussian 09 program. The optimized structures of CBTA and CBTA- $\text{CN}^-$  are displayed in Fig. S11 and S12 (ESI<sup>†</sup>) respectively. Fig. S13 and S14 (ESI<sup>†</sup>) display the contour plots of some selected molecular orbitals including HOMO and LUMO of CBTA and CBTA- $\text{CN}^-$  respectively. The HOMO–LUMO energy gap of CBTA (2.52 eV) is considerably increased in CBTA- $\text{CN}^-$  (3.65 eV), which implies the shifting of high energy bands in the adduct, thereby correlating the appearance of a new band at a shorter

Table 1 Recovery experiment for various natural water samples using the proposed methods

Source	Sample	CN added (mol l <sup>-1</sup> )	CN recovery (mol l <sup>-1</sup> ) <sup>a</sup>	Recovery (%)
Tap water	Tap water 1	0	Not detected	
	Tap water 2	$4.00 \times 10^{-4}$	$(3.96 \pm 0.04) \times 10^{-4}$	99
	Tap water 3	$3.00 \times 10^{-3}$	$(2.93 \pm 0.03) \times 10^{-3}$	97
Pond water	Pond water 1	0	Not detected	
	Pond water 2	$4.00 \times 10^{-4}$	$(3.94 \pm 0.03) \times 10^{-4}$	98.5
	Pond water 3	$3.00 \times 10^{-3}$	$(2.97 \pm 0.02) \times 10^{-3}$	99
River water	River water 1	0	Not detected	
	River water 2	$4.00 \times 10^{-4}$	$(4.02 \pm 0.06) \times 10^{-4}$	100.5
	River water 3	$3.00 \times 10^{-3}$	$(2.94 \pm 0.04) \times 10^{-3}$	98

<sup>a</sup> Relative standard deviations were calculated based on three times of measurement.

wavelength for the CBTA-CN<sup>-</sup> adduct, which is supported by the changes in the UV-visible spectra. In order to gain insights into the electronic transitions, the time-dependent density functional theory (TDDFT) was performed to the optimized geometries of the compounds, and the results are summarized in Table S1 (ESI†). The low energy transition for CBTA at 491 nm ( $\lambda_{\text{expt.}}$ , 410 nm) corresponds to HOMO → LUMO transition, while for CBTA-CN<sup>-</sup>, the low energy band shifted to 340 nm ( $\lambda_{\text{expt.}}$ , 353 nm) (Table S1, ESI†).

## Conclusion

In summary, a novel carbazole-based colorimetric and fluorometric sensor (CBTA) has been designed and successfully developed, which displayed the cyanide selective fluorescence 'ON-OFF' property. The receptor CBTA exhibited high selectivity, good sensitivity, rapid interaction time (within 22 s) and low LOD ( $7.68 \pm 0.29 \times 10^{-8}$  M for CN<sup>-</sup> detection in a 40% (v/v) DMSO-H<sub>2</sub>O mixture, which is very much lower than the WHO recommended value ( $1.9 \times 10^{-6}$  M) accompanied by the visual color changes from light yellow to colorless over other co-existing competitive anions. The quenching phenomenon of fluorescence intensity of the probe upon addition of CN<sup>-</sup> ions was explained to intra-molecular charge transfer (ICT) process, which is blocked by the nucleophilic attack of CN<sup>-</sup>, resulting in the discontinuance of  $\pi$ -conjugation that causes the observed photophysical changes and the findings were also supported by DFT calculations. Moreover, the excellent test strip response in the solid state helps us to detect CN<sup>-</sup> quantitatively without any sophisticated equipment. Therefore, the chemodosimeter CBTA can be served as a promising alternative for the selective recognition of cyanide in a mixed DMSO-H<sub>2</sub>O medium.

## Experimental section

### Materials and instrumentations

All the reagents, organic chemicals and solvents used in this synthesis such as 9H-carbazole, 4-fluorobenzaldehyde, 2-aminothiophenol, malononitrile, piperidine and potassium tert-butoxide were purchased from Sigma Aldrich and used without further purification. All spectroscopic grade solvents were from other commercial sources and used with no additional refinement. <sup>1</sup>H and <sup>13</sup>C NMR spectra were recorded using a Bruker 300 MHz instrument and DMSO-d<sub>6</sub> was used as a solvent using TMS as the internal standard. The chemical shifts are reported as  $\delta$  in units of parts per million (ppm). HRMS mass spectra were confirmed using a Waters (Xevo G2 Q-TOF) mass spectrometer. Elemental analysis was carried out using a 2400 Series-II CHN analyzer, PerkinElmer, USA. A PerkinElmer Lambda 750 spectrophotometer was used to obtain absorbance spectra and emission property was measured using a Shimadzu RF-6000 fluorescence spectrophotometer at room temperature (298 K). Lifetimes were measured using a time-resolved spectrofluorometer from IBH, UK.

### UV-vis and fluorescence method

For UV-vis titrations, a stock solution of the probe, CBTA (10  $\mu$ M), was prepared in DMSO/H<sub>2</sub>O, 40:60, v/v at 25 °C using a HEPES buffered solution. Deionized water was used to make all the solutions of guest anions using their sodium salts ( $1 \times 10^{-5}$  M) and the solution of cyanide ion using tetra butyl ammonium cyanide salt using HEPES buffer at physiological pH. The solutions of different concentrations of the receptor and all the anions were prepared separately and then the spectra of these solutions were recorded by the UV-vis method. Similarly, for fluorescence titrations, stock solutions were prepared using similar procedures and then the spectra were recorded by a fluorescence method.

### Measurement of fluorescence at different pH

For pH study, stock solution of the probe, CBTA (10  $\mu$ M) was prepared in DMSO/H<sub>2</sub>O, 40:60, v/v at 25 °C using a HEPES buffer solution. The pH was adjusted by an aqueous solution of 1 M HCl and 1 M NaOH. The solutions of probe and different concentrations of acids and bases were prepared separately by adjusting pH and the spectra of these solutions were recorded by a fluorescence technique. A similar study was executed while recording the pH titration of the probe (CBTA) in the presence of CN<sup>-</sup>.

### (E)-3-(4-(9H-carbazol-9-yl)phenyl)-2-(benzo[d]thiazol-2-yl)acrylonitrile (CBTA)

4-(9H-Carbazol-9-yl)benzaldehyde<sup>72</sup> and 2-(benzo[d]thiazol-2-yl)acetonitrile<sup>73</sup> were synthesized by following the procedure reported previously. 2-(Benzo[d]thiazol-2-yl)acetonitrile (0.09 gm, 0.52 mmol) and piperidine (0.52 mmol) were added to the stirred ethanolic solution of 4-(9H-carbazol-9-yl)benzaldehyde (0.141 gm, 0.52 mmol) and the whole mixture was stirred under refluxing condition for 8 hours in an inert atmosphere. After completion of the reaction, the reaction mixture was allowed to cool and the yellow precipitation was collected by filtration. The product was purified by column chromatography to get the final product. Yield was, 0.363 g, 85%.

<sup>1</sup>H NMR (300 MHz, DMSO-d<sub>6</sub>).  $\delta$  (ppm) 8.57 (s, 1H), 8.42 (d, 2H,  $J = 8.5$  Hz), 8.22–8.3 (m, 3H), 8.13 (d, 1H,  $J = 7.9$  Hz), 7.93 (d, 2H,  $J = 8.4$  Hz), 7.56–7.63 (m, 4H), 7.49 (t, 2H,  $J = 8$  Hz), 7.35 (t, 2H,  $J = 7.4$  Hz).

<sup>13</sup>C NMR (75 MHz, DMSO-d<sub>6</sub>).  $\delta$  (ppm) 49.0, 105.9, 110.4, 116.6, 121.2, 123.0, 123.7, 127.0, 127.7, 131.3, 132.6, 134.8, 139.9, 140.6, 147.6, 153.3, 163.6.

HRMS. Calculated for C<sub>28</sub>H<sub>18</sub>N<sub>3</sub>S [MH]<sup>+</sup>, ( $m/z$ ) = 428.1221; found = 428.1207.

### Theoretical study

All the calculations were performed using the Gaussian 09 program package.<sup>74</sup> The density functional theory (DFT) was used for the full geometry optimization at the B3LYP<sup>75,76</sup> level for the compounds. The calculations were aided using the Gauss View visualization program. All elements except aluminium were assigned by the 6-31+G(d)<sup>77</sup> basis set. The vibrational frequency

calculations were executed to assure that the optimized geometries stand for the local minima and there were only positive eigen values. Vertical electronic excitations based on B3LYP optimized geometries were computed using the time-dependent density functional theory (TDDFT) formalism<sup>78–80</sup> in methanol using a conductor-like polarizable continuum model (CPCM).<sup>81–83</sup>

## Conflicts of interest

There are no conflicts to declare.

## Acknowledgements

Authors thank CSIR (No. 01(2992)/19/EMR-II) and SERB (No. No. EEQ/2018/000266), New Delhi, India for financial supports.

## Notes and references

- J. M. Holloway, R. A. Dahlgren, B. Hansen and W. H. Casey, *Nature*, 1998, **395**, 785.
- D. Cheng, H. H. Ngo, W. Guo, S. W. Chang, D. D. Nguyen, Y. Liu, Q. Wei and D. Wei, *J. Hazard. Mater.*, 2020, **387**, 121682.
- M. E. Mahmoud, M. F. Amira, S. M. Seleim and A. K. Mohamed, *J. Hazard. Mater.*, 2020, **381**, 120979.
- I. Zwolak, *Biol. Trace Elem. Res.*, 2020, **193**(1), 44–63.
- B. Zuo, Q. Deng, H. Shao, B. Cao, Y. Fan, W. Li and M. Huang, *ACS Appl. Nano Mater.*, 2021, **4**(2), 1831–1840.
- B. Zuo, W. Li, X. Wu, S. Wang, Q. Deng and M. Huang, *Chem. – Asian J.*, 2020, **15**(8), 1248–1265.
- F. Wang, L. Wang, X. Chen and J. Yoon, *Chem. Soc. Rev.*, 2014, **43**, 4312–4324.
- M. D. Sobsey and S. Bartram, *Forum Nutr.*, 2003, **56**, 396–405.
- D. A. Jones, *Phytochem.*, 1998, **47**, 155–162.
- M. Zagrobelny, S. Bak and B. L. Moller, *Phytochem.*, 2008, **69**, 1457–1468.
- D. G. Barceloux, *Disease-a-Month*, 2009, **55**, 336–352.
- U. A. Patrick, N. Egwuonwn and A. A. Onunkwo, *J. Soil Sci. Environ. Manage.*, 2011, **2**, 49–57.
- I. F. Bolarinwa, C. Orfila and M. R. Morgan, *Food Chem.*, 2014, **152**, 133–139.
- L. D. Tivana, J. D. C. Francisco, F. Zelder, B. Bergenstahl and P. Dejmek, *Food Chem.*, 2014, **158**, 20–27.
- M. T. Wilson, G. Antonini, F. Malatesta, P. Sarti and M. Brunori, *J. Biol. Chem.*, 1994, **269**, 24114–24119.
- A. V. Gourine, N. Dale, E. Liaudet, D. M. Poputnikov, K. M. Spyer and V. N. Gourine, *J. Physiol.*, 2007, **585**, 305–316.
- S. H. Park, N. Kwon, J. H. Lee, J. Moon and I. Shin, *Chem. Soc. Rev.*, 2020, **49**, 143–179.
- X. Lv, J. Liu, Y. Zhao, M. Chen, P. Wang and W. Guo, *Org. Biomol. Chem.*, 2011, **9**, 4954–4958.
- A. Ishizaki, T. R. Calhoun, G. S. Schlaucohen and G. R. Fleming, *Phys. Chem. Chem. Phys.*, 2010, **12**, 7319–7337.
- K. Xiong, F. Huo, C. Yin, Y. Yang, J. Chao, Y. Zhang and M. Xu, *Sens. Actuators, B*, 2015, **220**, 822–828.
- Z. Liu, X. Wang, Z. Yang and W. He, *J. Org. Chem.*, 2011, **76**, 10286–10290.
- S. Goswami, S. Paul and A. Manna, *Tetrahedron Lett.*, 2014, **55**, 3946–3949.
- A. C. Sedgwick, L. Wu, H. H. Han, S. D. Bull, X. P. He, T. D. James, J. L. Sessler, B. Z. Tang, H. Tian and J. Yoon, *Chem. Soc. Rev.*, 2018, **47**, 8842–8880.
- W. H. Ding, D. Wang, X. L. Zheng, W. J. Ding, J. Q. Zheng, W. H. Mu, W. Cao and L. P. Jin, *Sens. Actuators, B*, 2015, **209**, 359–367.
- M. Jamkratoke, V. Ruangpornvisuti, G. Tumcharern, T. Tuntulani and T. Tomapatanaget, *J. Org. Chem.*, 2009, **74**, 3919–3922.
- C. R. Wade and F. P. Gabbai, *Inorg. Chem.*, 2010, **49**, 714–720.
- Q. Zou, F. Tao, Z. Xu, Y. Ding, Y. Tian and Y. Cui, *Anal. Methods*, 2019, **11**, 5553–5561.
- H. Wu, M. Chen, Q. Xu, Y. Zhang, P. Liu, W. Li and S. Fan, *Chem. Commun.*, 2019, **55**, 15137–15140.
- K. Vongnam, K. Chansaenpak, M. Sukwattanasinitt and P. Rashatasakhon, *ChemistrySelect*, 2020, **5**, 4303–4306.
- R. Dalapati, S. Nandi and S. Biswas, *Dalton Trans.*, 2020, **49**, 8684–8692.
- D. Tamilarasan, R. Suhasini, V. Thiagarajan and R. Balamurugan, *Eur. J. Org. Chem.*, 2020, 993–1000.
- H. Fang, W. J. Qu, H. H. Yang, J. X. He, H. Yao, Q. Lin, T. B. Wei and Y. M. Zhang, *Dyes Pigm.*, 2020, **174**, 108066.
- G. Sun, W. Chen, Y. Liu, X. Jin, Z. Zhang and J. Su, *Dyes Pigm.*, 2020, **176**, 108224.
- A. Popczyk, Y. Cheret, A. El-Ghayoury, B. Sahraoui and J. Mysliwiec, *Dyes Pigm.*, 2020, **177**, 108300.
- L. Hou, F. Li, J. Guo, X. Zhang, X. Kong, X. T. Cui, C. Dong, Y. Wang and S. Shuang, *J. Mater. Chem. B*, 2019, **7**, 4620–4629.
- X. Zhao, Y. Sun, Y. Zhu, H. Chen, Z. Wang, S. Zhao, D. Cao and G. Liu, *J. Photochem. Photobiol., A*, 2018, **367**, 83–88.
- A. Ozdemir and S. Erdemir, *J. Photochem. Photobiol., A*, 2020, **390**, 112328.
- T. S. Reddy and M. S. Choi, *J. Photochem. Photobiol., A*, 2018, **351**, 108–114.
- J. Mei, N. L. C. Leung, R. T. K. Kwok, J. W. Y. Lam and B. Z. Tang, *Chem. Rev.*, 2015, **115**, 11718–11940.
- Y. Hong, J. W. Y. Lam and B. Z. Tang, *Chem. Soc. Rev.*, 2011, **40**, 5361.
- H. T. Feng, Y. X. Yuan, J. B. Xiong, Y. S. Zheng and B. Z. Tang, *Chem. Soc. Rev.*, 2018, **47**, 7452–7476.
- N. Zhao, C. Ma, W. Yang, W. Yin, J. Wei and N. Li, *Chem. Commun.*, 2019, **55**, 8494–8497.
- X. Wei, M. Zhu, H. Yan, C. Lu and J. Xu, *Chem. – Eur. J.*, 2019, **25**, 12671–12683.
- G. Jin, R. He, Q. Liu, M. Lin, Y. Dong, K. Li, B. Z. Tang, B. Liu and F. Xu, *Theranostics*, 2019, **9**, 246–264.
- Y. Li, K. Xu, Y. Si, C. Yang, Q. Peng, J. He, Q. Hu and K. Li, *Dyes Pigm.*, 2019, **171**, 107682.

- 46 J. Shi, Q. Deng, C. Wan, M. Zheng, F. Huang and B. Tang, *Chem. Sci.*, 2017, **8**, 6188–6195.
- 47 M. H. Chua, K. W. Shah, H. Zhou and J. Xu, *Molecules*, 2019, **24**(15), 2711.
- 48 T. Ghosh, S. Mitra, S. K. Maity and D. K. Maiti, *ACS Appl. Nano Mater.*, 2020, **3**(4), 3951–3959.
- 49 K. Santhiya, S. K. Sen and R. Natarajan, *Dyes Pigm.*, 2021, **185**, 108891.
- 50 Y. Wang, H. Liu, Z. Chen and S. Pu, *Spectrochim. Acta, Part A*, 2021, **245**, 118928.
- 51 Y. Liu, A. Qin and B. Z. Tang, *Prog. Polym. Sci.*, 2018, **78**, 92.
- 52 S. Bozkurt and E. Halay, *Tetrahedron*, 2020, **76**, 131647.
- 53 E. Keles, B. Aydinlerand and Z. Seferoğlu, *Curr. Org. Chem.*, 2023, **20**, 61.
- 54 D. Jothi, S. Munusamy, S. M. Kumar, S. Enbanathan and S. K. Iyer, *RSC Adv.*, 2022, **12**, 8570.
- 55 A. Tigreros and J. Portilla, *Eur. J. Org. Chem.*, 2022, e202200249.
- 56 X. Yang, X. Chen and X. Lu, *J. Mater. Chem. C*, 2016, **4**, 383–390.
- 57 H. Tavallali, G. Deilamy-Rad, A. Parhami and S. Kiyani, *Spectrochim. Acta, Part A*, 2014, **121**, 139–146.
- 58 T. D. Ashton, K. A. Jolliffe and F. M. Pfeffer, *Chem. Soc. Rev.*, 2015, **44**, 4547–4595.
- 59 N. H. Evans and P. D. Beer, *Angew. Chem., Int. Ed.*, 2014, **53**, 11716–11754.
- 60 A. Liu, R. Ji and S. L. Shen, *New J. Chem.*, 2017, **41**, 10096–10100.
- 61 Y. Feng, S. Li and D. Li, *Sens. Actuators, B*, 2017, **254**, 282–290.
- 62 Y. Ge, P. Wei and T. Wang, *Sens. Actuators, B*, 2018, **254**, 314–320.
- 63 Y. Wang, W. Shu and B. Han, *New J. Chem.*, 2017, **41**, 9262–9267.
- 64 X. Chen, L. Wang, X. Yang and L. Tang, *Sens. Actuators, B*, 2017, **241**, 1043–1049.
- 65 W. C. Lin and J. W. Hu, *Anal. Chim. Acta*, 2015, **893**, 91–100.
- 66 S. OğuzTümay, A. Şenocak and A. Mermer, *New J. Chem.*, 2021, **45**, 18400–18411.
- 67 S. Cheng, A. Li, X. Pan, H. Wang, C. Zhang, J. Li and X. Qi, *Anal. Bioanal. Chem.*, 2021, **413**, 4441–4450.
- 68 X. Pan, S. Cheng, C. Zhang and X. Qi, *Anal. Bioanal. Chem.*, 2020, **412**, 6959–6968.
- 69 J. Li, X. Qi, W. Wei, Y. Liu, X. Xu, Q. Lin and W. Dong, *Sens. Actuators, B*, 2015, **220**, 986–991.
- 70 L. Li, T. Yang, J. Yang and X. Zhang, *Sens. Actuators, B*, 2022, **353**, 131038.
- 71 R. Bhaskar and S. Sarveswari, *Inorg. Chem. Commun.*, 2019, **102**, 83–89.
- 72 B. Patil, J. Lade, S. Chiou, Y. Cheng, Y. Lin, Y. Jadhav, P. Chetti, C. Chang and A. Chaskar, *Org. Electron.*, 2021, **92**, 106090.
- 73 L. Patra, K. Aich, S. Gharami and T. K. Mondal, *J. Lumin.*, 2018, **201**, 419–426.
- 74 M. J. Frisch, G. W. Trucks, H. B. Schlegel, G. E. Scuseria, M. A. Robb, J. R. Cheeseman, G. Scalmani, V. Barone, B. Mennucci, G. A. Petersson, H. Nakatsuji, M. Caricato, X. Li, H. P. Hratchian, A. F. Izmaylov, J. Bloino, G. Zheng, J. L. Sonnenberg, M. Hada, M. Ehara, K. Toyota, R. Fukuda, J. Hasegawa, M. Ishida, T. Nakajima, Y. Honda, O. Kitao, H. Nakai, T. Vreven, J. A. Montgomery, Jr., J. E. Peralta, F. Ogliaro, M. Bearpark, J. J. Heyd, E. Brothers, K. N. Kudin, V. N. Staroverov, R. Kobayashi, J. Normand, K. Raghavachari, A. Rendell, J. C. Burant, S. S. Iyengar, J. Tomasi, M. Cossi, N. Rega, J. M. Millam, M. Klene, J. E. Knox, J. B. Cross, V. Bakken, C. Adamo, J. Jaramillo, R. Gomperts, R. E. Stratmann, O. Yazyev, A. J. Austin, R. Cammi, C. Pomelli, J. W. Ochterski, R. L. Martin, K. Morokuma, V. G. Zakrzewski, G. A. Voth, P. Salvador, J. J. Dannenberg, S. Dapprich, A. D. Daniels, Ö. Farkas, J. B. Foresman, J. V. Ortiz, J. Cioslowski and D. J. Fox, *Gaussian 09, Revision D.01*, Gaussian, Inc., Wallingford CT, 2009.
- 75 A. D. Becke, *J. Chem. Phys.*, 1993, **98**, 5648.
- 76 C. Lee, W. Yang and R. G. Parr, *Phys. Rev. B: Condens. Matter Mater. Phys.*, 1988, **37**, 785.
- 77 F. Furche and R. Ahlrichs, *J. Chem. Phys.*, 2002, **117**, 7433.
- 78 R. Bauernschmitt and R. Ahlrichs, *Chem. Phys. Lett.*, 1996, **256**, 454.
- 79 R. E. Stratmann, G. E. Scuseria and M. J. Frisch, *J. Chem. Phys.*, 1998, **109**, 8218.
- 80 M. E. Casida, C. Jamorski, K. C. Casida and D. R. Salahub, *J. Chem. Phys.*, 1998, **108**, 4439.
- 81 V. Barone and M. Cossi, *J. Phys. Chem. A*, 1998, **102**, 1995.
- 82 M. Cossi and V. Barone, *J. Chem. Phys.*, 2001, **115**, 4708.
- 83 M. Cossi, N. Rega, G. Scalmani and V. Barone, *J. Comput. Chem.*, 2003, **24**, 669.